Journal of Nuclear Medicine, published on May 10, 2017 as doi:10.2967/jnumed.117.191452

Specific Imaging of Bacterial Infection using 6" -^{18}F-Fluoromaltotriose: A Second Generation PET Tracer Targeting the Maltodextrin Transporter in Bacteria

Gayatri Gowrishankar[1], Jonathan Hardy[2], Mirwais Wardak*[1], Mohammad Namavari*[1], Robert E. Reeves[3], Evgenios Neofytou[4] Ananth Srinivasan[1], Joseph C. Wu[1&4], Christopher H. Contag[2] and Sanjiv Sam Gambhir[1&5]

1. Department of Radiology, Stanford University School of Medicine, Stanford CA 94305
2. Department of Pediatrics, Stanford University School of Medicine, Stanford CA 94305
3. Thermo Fisher Scientific
4. Stanford Cardiovascular Institute, Stanford University School of Medicine, Stanford CA 94305
5. Department of Bioengineering, Stanford University School of Medicine, Stanford CA 94305

* These authors contributed equally to this study.

Corresponding author: Sanjiv Sam Gambhir, M.D., Ph.D., 318 Campus Drive, Stanford CA 94305, 650-725-2309 (W); 650-724-4948 (F), E-mail: sgambhir@stanford.edu

First author: Gayatri Gowrishankar, PhD, 318 Campus Drive, Stanford CA 94305,

650-725-3113 (V); 650-724-4948 (F), E-mail: gayatrig@stanford.edu

Financial statement: Part of the study was supported by the following grants: CIRM RT3-07798, CIRM DR2-05394, NIH R01 HL133272 and NIH T32 EB009035.

Words: 4697

Running title: Imaging bacterial infection

ABSTRACT

Purpose: 6”-^{18}F-fluoromaltotriose is a novel positron emission tomography (PET) tracer that can potentially be used to image and localize most bacterial infections, much like 2-deoxy-2-^{18}F-fluoro-D-glucose (^{18}F-FDG) has been used to image and localize most cancers. However, unlike ^{18}F-FDG, 6”-^{18}F-fluoromaltotriose is not taken up by inflammatory lesions and appears to be specific to bacterial infections by targeting the maltodextrin transporter that is expressed in most Gram-positive and Gram-negative strains of bacteria. **Materials and Methods:** 6”-^{18}F-fluoromaltotriose was synthesized with high radiochemical purity and evaluated in several clinically relevant bacterial strains in cultures and in living mice. **Results:** 6”-^{18}F-fluoromaltotriose was taken up in both Gram-positive and Gram-negative bacterial strains. 6”-^{18}F-fluoromaltotriose was also able to detect *Pseudomonas aeruginosa* in a clinically relevant mouse model of wound infection. The utility of 6”-^{18}F-fluoromaltotriose to help monitor antibiotic therapies was also evaluated in rats. **Conclusions:** 6”-^{18}F-fluoromaltotriose is a promising new tracer that has significant diagnostic utility, with the potential to change the clinical management of patients suffering from infectious diseases of bacterial origin.

Key Words:

Infection imaging, Bacteria, 6”-^{18}F-fluoromaltotriose, PET/CT imaging

Subject Categories:

Infectious disease; Molecular imaging; PET/CT; Bacterial imaging; PET tracer

INTRODUCTION

Antimicrobial resistance as defined by the World Health Organization is the 'ability of bacteria to change such that the current regimen of antibiotics becomes ineffective' (*1*). In 2015 there were 480,000 new cases of multi-drug resistant (MDR) tuberculosis (*2*). A high proportion of hospital acquired infections are now attributed to methicillin resistant *Staphylococcus aureus* (MRSA) and other resistant forms of *E.coli*. A recent report from the Centers for Disease Control and Prevention (CDC) discussed this emerging public health crisis and estimated that antibiotic resistance added about $20 billion in excess direct health care costs, not including the additional costs to society in terms of lost productivity (*3,4*). Among the many measures advocated by the CDC to combat this crisis, there was a call for the development of novel diagnostics to detect and therefore help manage the treatment of infectious diseases. The traditional approach to diagnosing a bacterial infection involves biopsy of the infected tissue and/or blood and culture of the pathogenic microorganisms in defined microbiological media. Advances in bacterial genomics and 16s ribosomal RNA sequencing have bolstered this approach and improved our ability to identify the nature of the pathogen causing the disease (*5*).

Imaging, particularly nuclear medicine, has always played an important role in the diagnosis of infectious diseases. The use of ^{67}Ga-citrate, ^{18}F-FDG and labeled leukocytes has been well documented (*6-8*). Unfortunately, none of these tracers are specific for bacteria and are therefore unable to distinguish bacterial infection from sterile inflammation. Recent years have seen the development of several novel positron emission tomography (PET) tracers, including ^{68}Ga-Ubiquicidin and 1-2′-deoxy-2′-fluoro-β-D-arabinofuranosyl)-5-[^{124}I] iodouracil (FIAU) (*9-11*). Of these, ^{68}Ga-Ubiquicidin has shown promise in pre-clinical studies (*11*) but further evaluation

in multi-center clinical trials is warranted.(*11,12*). Other tracers including ^{18}F-Fluorodeoxysorbitol (FDS) have been shown to detect only a specific class of bacteria (for example, Gram-negative Enterobacteriaceae) (*13*). We have previously demonstrated the development of 6-[^{18}F]-fluoromaltose (Supplemental Fig 1), a probe from a novel class of tracers targeting the maltodextrin transporter in bacteria (*14,15*). The concept of this class of tracers stems from an earlier study by Murthy et al., who showed that the maltodextrin transporter is unique to bacteria and that a fluorescently labeled maltohexose probe was able to image *E. coli* induced myositis in rats (*16*). The maltose/maltodextrin transporter belongs to the ATP-binding cassette (ABC) family of transporters. Extensively studied in *E. coli*, this transporter system has been shown to be present in many bacterial species, both Gram-positive and Gram-negative, including *Enterococcus faecalis*, *Staphylococcus aureus*, *Streptococcus pneumoniae*, *Bacillus subtilis*, *Listeria monocytogenes* and *Vibrio cholera* (*17*). It has also been implicated in the virulence mechanisms of some of these pathogens (*18-21*). The transporter is a complex of five proteins with the outer membrane maltoporin (LamB) and the periplasmic maltose binding protein (MalE) serving as the key determinants of transporter specificity (*17*). The transporter appears to be somewhat promiscuous and has been reported to take up a wide variety of maltose analogs, which has benefited tracer design (*22*).

Murthy et al. reported the development of a tracer based on the ^{18}F labeled maltohexose (MH^{18}F) (Supplemental Fig 1) (*23*). Both our prior study and the work from Murthy et al. demonstrated that this class of tracers was not only specific for bacteria but could also accurately distinguish infection from sterile inflammation. However, both 6-^{18}F-fluoromaltose and MH^{18}F suffered from suboptimal pharmacokinetics and had poor signal-to-noise ratios, particularly in the thoracic region, which would preclude the use of these tracers for many clinical indications

including lung and cardiac infections. In an effort to clinically translate this class of tracers, we have developed an improved second-generation tracer, 6”-^{18}F-fluoromaltotriose, building on the same scaffold. The trisaccharide maltotrioses are also substrates for the maltodextrin transporter and are implicated in the virulence of bacterial pathogens including Group A *Streptococcus* (GAS) (*24*). In this study, we demonstrate that 6”-^{18}F-fluoromaltotriose is taken up by a variety of pathogenic bacterial strains *in vitro* and *in vivo*, and that its pharmacokinetic profile is superior to the previously characterized probes for the maltodextrin transporter.

MATERIALS AND METHODS

Synthesis:

6″-deoxy-6″-^{18}F-fluoro-α-D-glucopyranosyl-(1-4)-O-α-D-glucopyranosyl-(1-4)-O-D-glucopyranoside (6″-^{18}F-fluoromaltotriose) was prepared by nucleophilic displacement of the nosylate group in 2″,3″,4″-tri-O-acetyl-6″-deoxy-6″-O-nosyl-α-D-glucopyranosyl-(1-4)-O-(2′,3′,6′-tri-O-acetyl-α-D-glucopyranosyl-(1-4)-1,2,3,6 tetra-O-acetyl-D-glucopyranoside precursor by ^{18}Ffluoride ion in DMF (1 mL) at 85 ºC for 10 min. After cooling to room temperature, 10 mL of water was added and the solution passed through a light C-18 Sep-pack cartridge (Water) and the crude protected 6″-^{18}F-fluoromaltotriose removed by passing 3 mL of acetonitrile through the cartridge. The crude protected 6″-^{18}F-fluoromaltotriose was concentrated and deprotected first by 1N HCl (1mL) at 110 ºC for 10 min and then by 2N NaOH (0.5 mL) in room temperature for 5 min to afford crude 6″-^{18}F-fluoromaltotriose. After neutralization and HPLC purification of the solution, 6″-^{18}F-fluoromaltotriose was recovered in 6-9% radiochemical yield (decay corrected) with the 95% radiochemical purity.

Cultures

E. coli was obtained from American Type Culture Collections (ATCC 33456). The bioluminescent strain of *Pseudomonas aeruginosa* (Xen 5) and *Staphylococcus aureus* (Xen 36) were obtained from Perkin Elmer. The mammalian cell lines HCC1806 and HCC827 (breast and lung cancer cell lines) were obtained from ATCC and were grown in media recommended by ATCC.

Bacterial Uptake Studies

Bacterial uptake studies were performed as described in our previous publication (*14*). In brief, an overnight (O/N) culture of the respective strain of bacteria was initiated by inoculating a colony from a plate into a 3mL culture of LB broth. The next morning, 500 µL of the O/N culture was inoculated into 30 mL of LB in a 200 mL flask and grown in a 37ºC shaker/incubator until the bacterial culture reached log phase (OD_{600} = 0.5). Aliquots of 10^8 colony-forming units (CFU) of the bacterial culture were incubated with 0.37MBq of the tracer for the designated periods. At the end of the incubation period, unbound tracer was removed by washing and the cultures were lysed using a bacterial lysis solution (BugBuster, EMD, Billerica MA USA). The counts associated with the lysate were determined using a gamma counter. The protein concentration in the lysate was determined using BCA (Pierce, Thermo Fisher Scientific, Rockford IL, USA). All samples were compared to total activity references and the percentage uptake per microgram of protein (%uptake/µg protein) was calculated.

***E.Coli* Induced Murine Myositis**

All animal models were approved by the Stanford University Institutional Animal Care and Use Committee .6-7 week old nude mice (n = 4) were anesthetized by isoflurane inhalation. 1 x 10^8 (colony forming units) CFU of a specific strain of *E.coli* (ATCC 33456) in 50µL of LB broth was administered, as an intra-muscular injection, into the right thigh of the mice as described previously (*14*). The mice were imaged 24h after the initial infection.

Pseudomonas aeruginosa Wound Infection Model

8 week old CD1 mice (n=8) were anesthetized by isoflurane inhalation. A small wound was made on the back of the mice using a sharp pair of scissors. 10^6 CFU of Xen 5, a bioluminescent strain of *Pseudomonas aeruginosa,* in 20 μL of saline was inoculated into a small pocket just under the skin beneath the wound. The wound was then sealed with Vetbond (3M 1469SB) adhesive. The mice were imaged 24h after the infection.

Listeria Monocytogenes Model

8 week old CD1 mice (n=5), were infected intravenously with $2x10^5$ CFU of the bioluminescent *L. monocytogenes* strain Xen 32. BLI was performed the next day as described above. The mice were imaged laterally on the left side to reveal splenic signal characteristic of listeriosis in CD1 mice. At this dose, the infection is lethal in 3-5 days.

Lipopolysaccharide (LPS) Lung Inflammation Model

6-7 week old BALB/c mice were anesthetized by isoflurane inhalation. 50 μg of lipopolysaccharide (from Escherichia coli serotype 0127:B8, Sigma) in 20 μL of saline (0.9% NaCl) was administered via intranasal instillation (Rignault S et al, Shock 2007). The control group consisted of mice without any treatment since simple administration of vehicle (saline) is enough to induce lung inflammation. 24h after LPS administration, the mice were sacrificed for biodistribution studies and the lungs were saved for histopathological analysis.

Heat Inactivation of *E. Coli*

An O/N culture of the same strain of *E. coli* was set up as described above and allowed to reach log phase. Aliquots of the culture containing 10^6, 10^7 or 10^8 CFU of bacteria were heat

inactivated at 90˚C for 30 minutes and then implanted in the left thigh of nude mice (n =3). An equal number of viable bacteria were implanted in the contralateral thigh by intra-muscular injection. 1 hour later the mice were imaged by micro PET/CT.

Bioluminescence Imaging

In vivo bioluminescence imaging (BLI) was performed using the IVIS Spectrum instrument (Perkin Elmer). The engineered bioluminescent strains of bacteria are able to synthesize their own substrate for the bacterial luciferase, so there was no need to administer substrate. The mice were positioned in the instrument after being anesthetized with isoflurane and imaged under large binning conditions for a suitable exposure time (up to 5 min).

Micro PET/CT

7.4 MBq of the radiotracer was administered to the mice intravenously as described previously (*14*). The mice were kept anesthetized with isoflurane after tracer administration. At the desired times, the mice were placed on the bed of the micro PET/CT scanner (Inveon, Siemens, Germany) and 5 min static scans were performed. For the dynamic scans, tail vein catheters (12cm PU tubing and 27g butterfly needle) were inserted into the tail vein of the mice and the catheter was glued onto the tail using Vet Bond (tissue glue). Once the animal was in position in the PET part of the PET/CT scanner, 7.4 MBq of the tracer was administered via the catheter and the PET scan was started. The dynamic scan was performed for an hour. During the scan, special precautions were taken to make sure the mice were warm. All images were reconstructed using 3D-OSEM. Region of interest (ROI) analysis were done using IRW software (Inveon Research Workplace, Siemens, Germany). No partial volume corrections were performed on the PET image data.

Biodistribution Studies

7.4 MBq of the radiotracer was administered to the rodents intravenously. The rodents were kept anesthetized after tracer administration. At the desired time after tracer injection, the mice were sacrificed by cervical dislocation. Then relevant organs/tissues were removed, placed in gamma counter tubes and weighed. Tissue-associated radioactivity was determined in a gamma counter (Cobra, Perkin Elmer, Waltham MA USA), decay-corrected to time of tracer injection and normalized to total injected activity using diluted aliquots of the initial administered dose as standards as described previously (*14*).

Histology

The tissues were collected in formalin, embedded in paraffin and processed. Hematoxylin & Eosin (H&E) staining of the lung sections was done using standard protocols.

Statistical Methods

Unpaired t test was performed to compare differences between control and treated groups using Graphpad from Prism (version 6.0, La Jolla CA, USA)

RESULTS

Uptake of 6"-^{18}F-Fluoromaltotriose in Bacterial Cultures

6"-^{18}F-fluoromaltotriose (see Supplemental Fig 1 for structure) was incubated with different strains of bacteria (Fig. 1A). As shown previously for our first generation tracer (*14*), 6"-^{18}F-fluoromaltotriose was taken up by both gram negative (*E. coli* and *P. aeruginosa*) and gram positive (*S. aureus* and *L. monocytogenes*) bacteria. The different strains of bacteria took up different amounts of 6"-^{18}F-fluoromaltotriose per cell, possibly reflecting the different expression levels of the maltodextrin transporter, as well as the physical size of the bacterial cell. The uptake of 6"-^{18}F-fluoromaltotriose was blocked by co-incubation with 1 mM of maltose, indicating that the tracer was being taken up through the maltose transport system (unpublished data). 6"- ^{18}F-fluoromaltotriose was not taken up by two mammalian cancer cell lines (Fig. 1C), as was also shown for the first generation maltose tracer (*14*). In contrast to our first generation disaccharide tracer, the new 6"-^{18}F fluoromaltotriose tracer was retained very well in *E.coli* cultures (50% retention vs. 5% retention; Supplemental Fig. 2).

6"-^{18}F-Fluoromaltotriose in *E. Coli* Induced Myositis in Living Mice

In a simple *E.coli* induced myositis model (see Methods), 6"-^{18}F-fluoromaltotriose was able to distinguish infected muscle from the uninfected contralateral muscle (3.4-fold, $p < 0.05$; Fig. 1B). 6"-^{18}F-fluoromaltotriose was also able to detect as little as 10^6 CFU of *E.coli* in mice (Fig. 2B). The tracer is taken up only in viable bacteria (shown by yellow arrow), as is its predecessor (Fig. 2B). There appears to be a modest correlation between the amount of tracer that was taken up and the number of implanted *E.coli* (Pearson $r = 0.61$, $p < 0.05$; Supplemental Fig. 3). Dynamic PET/CT scans acquired over the course of an hour showed excellent retention of 6"-

^{18}F-fluoromaltotriose in the infected muscle (Fig. 2A) in an *E.coli* induced myositis model with the maximum accumulation seen at 30 minutes post tracer administration. *Ex-vivo* biodistribution studies comparing 6-^{18}F-fluoromaltose and 6”-[^{18}F]-fluoromaltotriose showed a predominantly renal clearance with some clearance via the hepatobiliary system (Fig. 2C). 6”-^{18}F-fluoromaltotriose was not taken up differentially in an LPS induced lung inflammation model (1.04 fold difference between lungs of control and LPS treated mice; Figs. 3A and 3B), confirming its specificity for imaging bacterial infection.

6”-^{18}F-Fluoromaltotriose in a *Pseudomonas aeruginosa* Wound Infection Model

Pseudomonas aeruginosa is a well-known pathogen that often infects wounds and burns. It has also been notoriously difficult to image. In an effort to replicate a clinically relevant wound infection model, 10^6 CFU of Xen 5, a bioluminescent strain of *P. aeruginosa,* was inoculated into a superficial wound made into the back of immunocompetent mice (see Methods). Twenty-four hours later, bioluminescent (BLI) images of the mice were obtained, which confirmed the presence of viable bacteria (Fig. 4A). Micro PET/CT images obtained within 2 h (Fig. 4B) showed the accumulation of 6”-^{18}F-fluoromaltotriose in the infected wounds and little to no accumulation in the control mice wounds with phosphate buffered saline (PBS) administration. *Ex-vivo* biodistribution studies demonstrated a significant difference between infected and control wounds (4-fold difference, $p < 0.05$; Supplemental Fig. 4).

6”-^{18}F-Fluoromaltotriose in an Incidental *Staphylococcus aureus* Infection Model

A nude rat that developed an incidental bacterial infection post-cardiac surgery was imaged by microPET/CT following the administration of 6”-^{18}F-fluoromaltotriose via tail-vein. Necropsy of a similarly infected rat from the same group revealed extensive botryomycosis-like lesions due to

Staphylococcus aureus (data not shown). Botryomycosis is a bacterial infection characterized by granulomatous skin lesions filled with pus and bacteria. A 60-minute dynamic PET/CT scan was acquired on the rat revealing focal uptake of 6”-^{18}F-fluoromaltotriose in the thoracic region (Fig. 5, left panel), which was absent in the control rats (Fig. 5, right panel). The rat was then treated with Cefazolin, a broad-spectrum antibiotic, for one month and then imaged again on the microPET/CT scanner after tail-vein injection of 6”-^{18}F-fluoromaltotriose. The PET images obtained post-antibiotic therapy show a marked reduction in the uptake of the tracer in the thoracic region (Fig. 5, middle panel), confirming that the initial uptake was likely due to the presence of a bacterial infection.

DISCUSSION

In this study, we present data characterizing 6”-^{18}F-fluoromaltotriose, a novel tracer targeting the maltodextrin transporter of bacteria (see Supplemental Fig 8). This is a second-generation tracer and displays a marked improvement in its pharmacokinetic (PK) profile over the first generation tracer as shown in Figure 2C, undergoing predominantly renal clearance. This result is in contrast to our first generation tracer, 6-^{18}F- fluoromaltose, which displayed extensive hepatobiliary clearance (Fig. 2C and (*14*)). A head to head comparison of the biodistribution profiles of 6-^{18}F-fluoromaltose and 6”-^{18}F-fluoromaltotriose (Fig. 2C) showed that the maltotriose tracer also had reduced uptake in blood and muscle as compared to the maltose tracer, thereby boosting the target/background ratios significantly. The 6”-^{18}F-fluoromaltotriose tracer showed improved retention in *E.coli*, as shown in Supplemental Fig. 2 (50% vs 5% for the 6-^{18}F-fluoromaltose;) (*14*) indicating that perhaps the maltotriose is being metabolized to glucose at a slower rate than the maltose. This difference in metabolism could also permit the 6”-^{18}F-fluoromaltotriose to discriminate between bacterial and fungal infections. There is evidence that, although fungi can take up and metabolize maltose, maltotriose appears unique in that it is metabolized more slowly in yeast (*25*). More experiments with bacteria bearing mutations in the maltodextrin transporter are needed to truly understand the mechanism of uptake and utilization of the tracer.

The improved PK profile also leads to an improvement in sensitivity. As shown in Fig. 2B, 6”-^{18}F-fluoromaltotriose can pick up as few as 10^6 CFU of *E. coli* (infected tissues usually have 10^5-10^6 CFU of bacteria), with an improved SNR as compared to the first generation tracer 6-^{18}F-fluoromaltose (*14*). There is also evidence that tracers targeting the maltodextrin transporter can be taken up in *S. aureus* biofilms, as shown by Murthy et al. (*16*). This class of imaging agents

can therefore be used to image bacterial biofilm infections. While there has been a report on the use of ^{18}F-FDG to image *S. aureus* biofilms in mice (*26*), the use of 6"-^{18}F-fluoromaltotriose would enable imaging the biofilm infection rather than the surrounding inflammation. Bacterial biofilms have been implicated in the pathogenesis of a wide variety of chronic infections, particularly in patients that have had surgical implants or prosthetics (*27*). Other instances of chronic infections include cystic fibrosis patients who have lung infections very often attributed to *Pseudomonas aeruginosa* biofilms (*28*). Our data shows that 6"-^{18}F-fluoromaltotriose is taken up by *P. aeruginosa* both *in vitro* and *in vivo* in a wound infection model, and it is very likely that the tracer would be taken up in *P. aeruginosa* biofilms, which we hope to explore in the future. Additionally, this is the first and only report we know of in which an imaging agent is shown to be capable of detecting *P. aeruginosa* infections *in vivo* (both FIAU (*9*) and Fluorodeoxysorbitol (*13*) were not taken up by *P. aeruginosa*).

Maltotriose does not cross the blood brain barrier, so it cannot be used for imaging bacterial meningitis, nor can it be used to image infections caused by certain bacterial pathogens that may have an intracellular phase in their lifecycle (e.g., *Listeria monocytogenes*, *Salmonella typhimurium, Mycobacterium tuberculosis*). In the case of *L. monocytogenes,* we have observed in an *in vivo* infection model (Supplemental Figures 5,6 and 7) that 6"-^{18}F-fluoromaltotriose was able to detect the infection in mice that appeared to have widespread disseminated systemic infection, as observed by BLI (Supplemental Figure 5 and 6), and elevated uptake in blood Supplemental figure 7), which has been observed in a small percentage of infected animals in other studies (*29*). It may therefore be possible to image facultative intracellular pathogens such as *M. tuberculosis*, using 6"-^{18}F- fluoromaltotriose if some of the bacteria are extracellular. However, extensive studies would be required to explore such a possibility. In many ways, 6"-

^{18}F-fluoromaltotriose (and other tracers targeting the maltodextrin transporter) are conceptually similar to ^{18}F-FDG. Just as ^{18}F-FDG is internalized into cells and used in the diagnosis of most human cancers, 6”-^{18}F- fluoromaltotriose is internalized in several bacterial pathogens, both Gram-negative and Gram-positive (Fig. 1A). Also, just as ^{18}F-FDG cannot distinguish between different types of cancers, 6”-^{18}F-fluoromaltotriose cannot distinguish between different types of bacterial strains. Tracers under investigation, such as ^{18}F-fluorodeoxysorbitol and others (*30*) which are internalized by specific bacterial pathogens, might be used in conjunction to complete the diagnosis when clinically necessary. In contrast to ^{18}F-FDG, however, 6”-^{18}F-fluoromaltotriose can apparently distinguish infection from inflammation (Fig. 3B).

The study performed in rats (Fig. 5) confirms the PK profile observed in mice (predominantly renal), and also illustrates the potential utility of 6”-^{18}F-fluoromaltotriose in monitoring responses to antibiotic therapy. It also reflects the clinically relevant situation in which a severe infection must be treated and monitored without definitive identification of the pathogen. Although it is likely that the rat in question was infected with *S. aureus* as in the other similarly infected rat in the same group, this assumption was not verified and yet the imaging proved efficacious. Given the rise in antibiotic resistance, the use of imaging to guide the choice and duration of antibiotic treatment can help mitigate the emergence of resistance. This possibility becomes important in diseases such as tuberculosis and osteomyelitis, which involve prolonged use of antibiotics, because physicians may be unable to determine whether or not the bacterial infection has been successfully treated. While PET itself cannot replace emergent ‘point of care’ diagnostics as a screening tool for infectious diseases, 6”-[^{18}F]-fluoromaltotriose and other similar PET tracers in development will play a key role in the hospital setting to confirm,

localize and determine the spread of bacterial infection, particularly in the context of other confounding indications such as inflammation and cancer.

CONCLUSION

6”-^{18}F-fluoromaltotriose is the second in a series of tracers that are being developed targeting the bacterial maltodextrin transporter. The studies outlined above have demonstrated that the tracer is able to image bacterial infections in pre-clinical models and shown that the pharmacokinetic properties of this novel tracer make it suitable for future clinical studies. The tracer cannot be used to image infections caused by bacteria that invade cells eg, *Mycobacterium tuberculosis* which does limit the utility of the tracer.

DISCLOSURE

The authors have a patent on 6”-^{18}F-fluoromaltotriose. Patent title: PROBES AND METHODS OF IMAGING A BACTERIAL INFECTION; Serial No.: 15/096,308; Filing Date: April 12, 2016.

ACKNOWLEDGEMENTS

We acknowledge Dr. Frezghi Habte and the Stanford University Small Animal Imaging Facility for their help with the image analysis and quantitation. We are also grateful to the radiochemistry facility for their radiochemistry support. Moreover, we are deeply appreciative for the funding support from the following grants: CIRM RT3-07798, CIRM DR2-05394, NIH R01 HL133272 and NIH T32 EB009035.

REFERENCES:

1. Marston HD, Dixon DM, Knisely JM, Palmore TN, Fauci AS. Antimicrobial Resistance. *JAMA.* 2016;316:1193-1204.

2. Morens DM, Fauci AS. Emerging infectious diseases: threats to human health and global stability. *PLoS Pathog.* 2013;9:e1003467.

3. Antibiotic Resistant threats in the United States. In: US Department of Health and Human Services CfDCaP, ed; 2013.

4. National action plan for combating antibiotic resistant bacteria. In: The White House W, ed; 2015.

5. Janda JM, Abbott SL. 16S rRNA gene sequencing for bacterial identification in the diagnostic laboratory: pluses, perils, and pitfalls. *J Clin Microbiol.* 2007;45:2761-2764.

6. Sasser TA, Van Avermaete AE, White A, et al. Bacterial infection probes and imaging strategies in clinical nuclear medicine and preclinical molecular imaging. *Curr Top Med Chem.* 2013;13:479-487.

7. van Oosten M, Hahn M, Crane LM, et al. Targeted imaging of bacterial infections: advances, hurdles and hopes. *FEMS Microbiol Rev.* 2015;39:892-916.

8. Bunschoten A, Welling MM, Termaat MF, Sathekge M, van Leeuwen FW. Development and prospects of dedicated tracers for the molecular imaging of bacterial infections. *Bioconjug Chem.* 2013;24:1971-1989.

9. Peterson KL, Reid WC, Freeman AF, et al. The use of 14C-FIAU to predict bacterial thymidine kinase presence: implications for radiolabeled FIAU bacterial imaging. *Nucl Med Biol.* 2013;40:638-642.

10. Diaz LA, Jr., Foss CA, Thornton K, et al. Imaging of musculoskeletal bacterial infections by [124I]FIAU-PET/CT. *PLoS One.* 2007;2:e1007.

11. Ebenhan T, Zeevaart JR, Venter JD, et al. Preclinical evaluation of 68Ga-labeled 1,4,7-triazacyclononane-1,4,7-triacetic acid-ubiquicidin as a radioligand for PET infection imaging. *J Nucl Med.* 2014;55:308-314.

12. Vilche M, Reyes AL, Vasilskis E, Oliver P, Balter H, Engler H. (6)(8)Ga-NOTA-UBI-29-41 as a PET Tracer for Detection of Bacterial Infection. *J Nucl Med.* 2016;57:622-627.

13. Weinstein EA, Ordonez AA, DeMarco VP, et al. Imaging Enterobacteriaceae infection in vivo with 18F-fluorodeoxysorbitol positron emission tomography. *Sci Transl Med.* 2014;6:259ra146.

14. Gowrishankar G, Namavari M, Jouannot EB, et al. Investigation of 6-[(1)(8)F]-fluoromaltose as a novel PET tracer for imaging bacterial infection. *PLoS One.* 2014;9:e107951.

15. Namavari M, Gowrishankar G, Hoehne A, Jouannot E, Gambhir SS. Synthesis of [(1)(8)F]-labelled maltose derivatives as PET tracers for imaging bacterial infection. *Mol Imaging Biol.* 2015;17:168-176.

16. Ning X, Lee S, Wang Z, et al. Maltodextrin-based imaging probes detect bacteria in vivo with high sensitivity and specificity. *Nat Mater.* 2011;10:602-607.

17. Ferenci T. The recognition of maltodextrins by Escherichia coli. *Eur J Biochem.* 1980;108:631-636.

18. Gopal S, Berg D, Hagen N, et al. Maltose and maltodextrin utilization by Listeria monocytogenes depend on an inducible ABC transporter which is repressed by glucose. *PLoS One.* 2010;5:e10349.

19. Hanses F, Roux C, Dunman PM, Salzberger B, Lee JC. Staphylococcus aureus gene expression in a rat model of infective endocarditis. *Genome Med.* 2014;6:93.

20. Jones SA, Jorgensen M, Chowdhury FZ, et al. Glycogen and maltose utilization by Escherichia coli O157:H7 in the mouse intestine. *Infect Immun.* 2008;76:2531-2540.

21. Lang H, Jonson G, Holmgren J, Palva ET. The maltose regulon of Vibrio cholerae affects production and secretion of virulence factors. *Infect Immun.* 1994;62:4781-4788.

22. Ferenci T. Methyl-alpha-maltoside and 5-thiomaltose: analogs transported by the Escherichia coli maltose transport system. *J Bacteriol.* 1980;144:7-11.

23. Ning X, Seo W, Lee S, et al. PET imaging of bacterial infections with fluorine-18-labeled maltohexaose. *Angew Chem Int Ed Engl.* 2014;53:14096-14101.

24. Shelburne SA, 3rd, Sumby P, Sitkiewicz I, et al. Maltodextrin utilization plays a key role in the ability of group A Streptococcus to colonize the oropharynx. *Infect Immun.* 2006;74:4605-4614.

25. Zastrow CR, Hollatz C, de Araujo PS, Stambuk BU. Maltotriose fermentation by Saccharomyces cerevisiae. *J Ind Microbiol Biotechnol.* 2001;27:34-38.

26. Garrido V, Collantes M, Barberan M, et al. In vivo monitoring of Staphylococcus aureus biofilm infections and antimicrobial therapy by [18F]fluoro-deoxyglucose-MicroPET in a mouse model. *Antimicrob Agents Chemother.* 2014;58:6660-6667.

27. Bjarnsholt T, Alhede M, Alhede M, et al. The in vivo biofilm. *Trends Microbiol.* 2013;21:466-474.

28. Trostrup H, Thomsen K, Christophersen LJ, et al. Pseudomonas aeruginosa biofilm aggravates skin inflammatory response in BALB/c mice in a novel chronic wound model. *Wound Repair Regen.* 2013;21:292-299.

29. Merrick JC, Edelson BT, Bhardwaj V, Swanson PE, Unanue ER. Lymphocyte apoptosis during early phase of Listeria infection in mice. *Am J Pathol.* 1997;151:785-792.

30. Ordonez AA, Weinstein EA, Bambarger LE, et al. A Systematic Approach for Developing Bacteria-Specific Imaging Tracers. *J Nucl Med.* 2017;58:144-150.

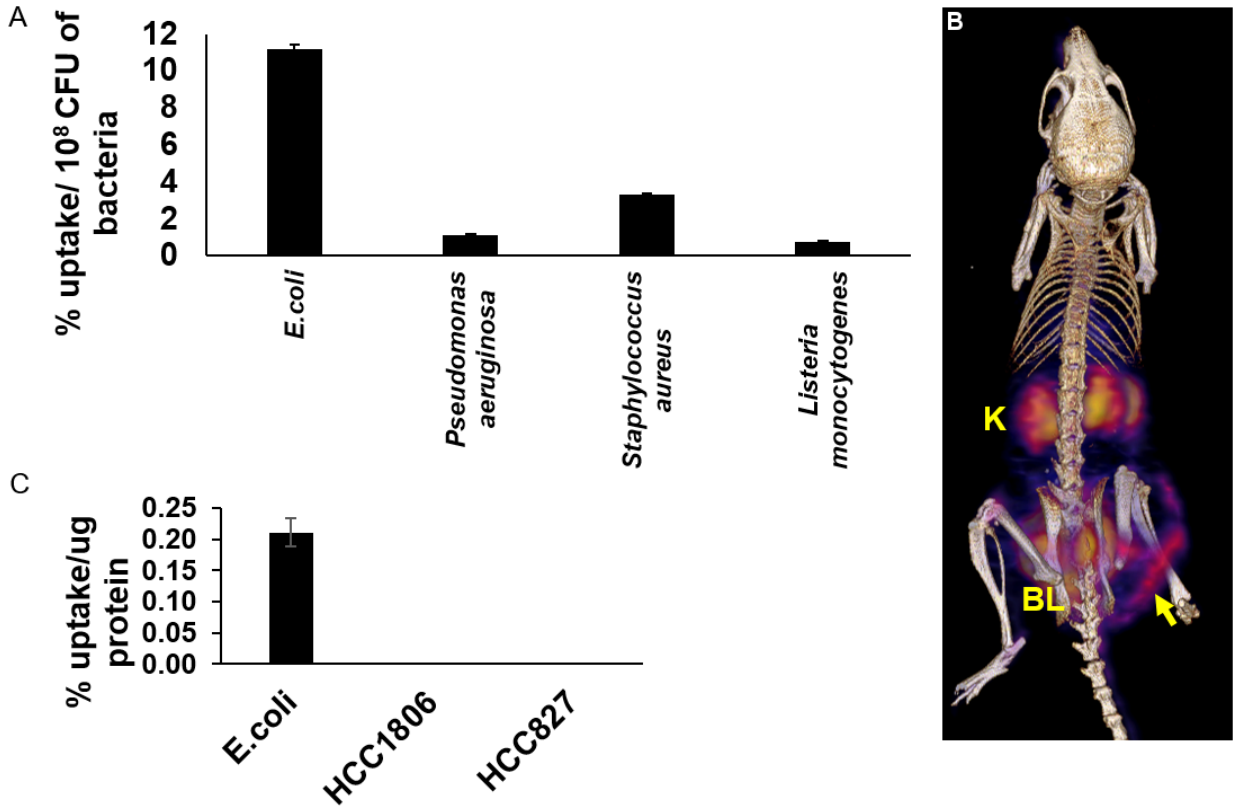

Figure 1: Evaluation of 6"-^{18}F-fluoromaltotriose in bacterial cultures and in mice: A) Uptake of 6"-^{18}F-fluoromaltotriose in the indicated strains of bacteria for 30 minutes. B) 3D color map from a micro PET/CT scan of a representative nude mouse with an *E.coli* infection in its right thigh 24h after infection and 1h after the intravenous injection of 7.4MBq of 6"-^{18}F fluoromaltotriose. Also seen in the image is the bladder (BL), kidneys (K). Yellow arrow highlights site of infection. C) Uptake of 6"-^{18}F-fluoromaltotriose in *E.co*li versus mammalian cancer cell lines-HCC1806 and HCC827. Error bars are standard deviation of means of triplicate samples.

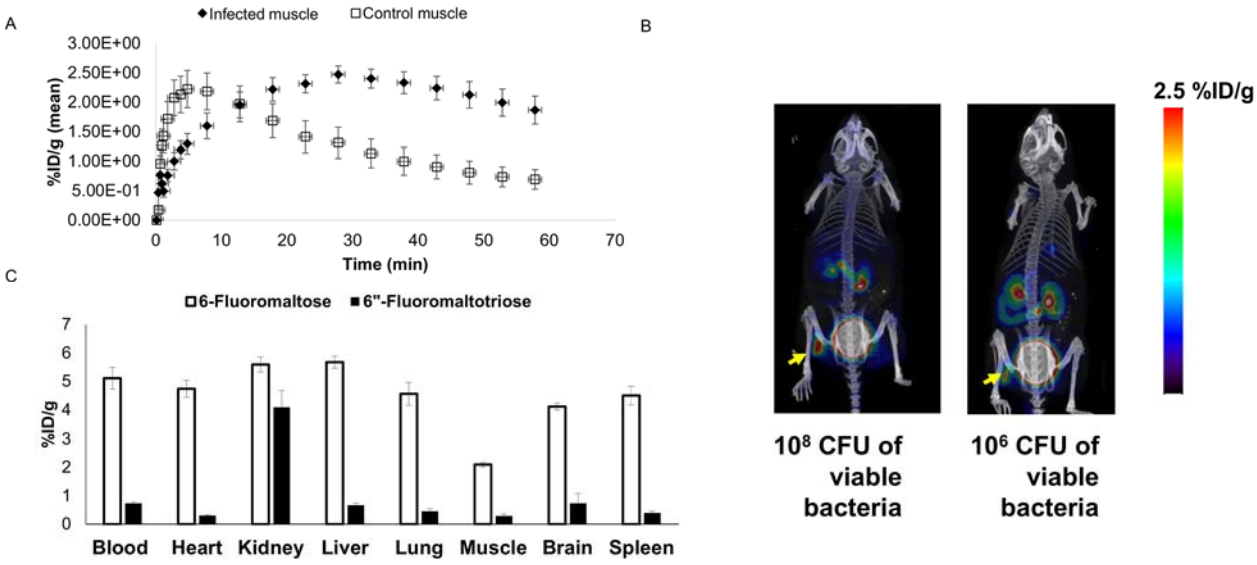

Figure 2: Evaluation of 6”-^{18}F-fluoromaltotriose in *E.coli* induced myositis: A) Time activity curve from a 1h dynamic micro PET/CT scan of mice (n =4) showing the accumulation of 6”-^{18}F-fluoromaltotriose in *E.coli* infected muscle. B) Maximum intensity projections from micro PET/CT of representative mice bearing 10^8 and 10^6 CFU of viable E.coli in the left muscle and the same number of heat inactivated bacteria in the right muscle, 1 hour after intravenous administration of the tracer. C) Ex-vivo bio-distribution comparing 6-^{18}F-fluoromaltose (light gray bars) (n=3) and 6”-^{18}F-fluoromaltotriose (black bars) (n=3) in nude mice, 1h after administration of tracer. Error bars represent standard deviation Error bars represent standard deviation of means.

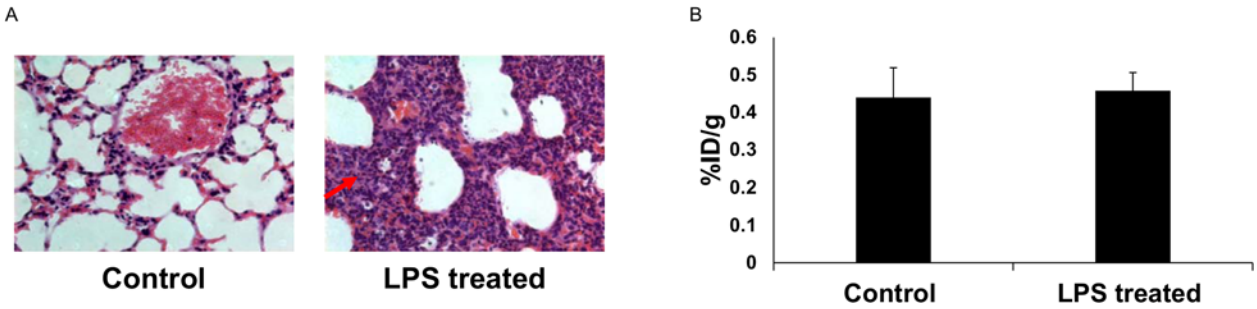

Figure 3: Evaluation of 6”-^{18}F-fluoromaltotriose in inflammation: A) Representative H&E stained sections of formalin fixed lungs from control mice (left panel) and from mice with LPS induced lung inflammation (right panel) showing thickening of the bronchial walls (red arrow) due to accumulation of neutrophils and macrophages (stained blue). B) Ex-vivo biodistribution quantitation of lungs from immunocompetent control mice (n=5) and mice after LPS induced lung inflammation (n=5), 24h after the administration of LPS intranasally and 1h after intravenous administration of 6”-^{18}F-fluoromaltotriose . Error bars represent standard deviation of means

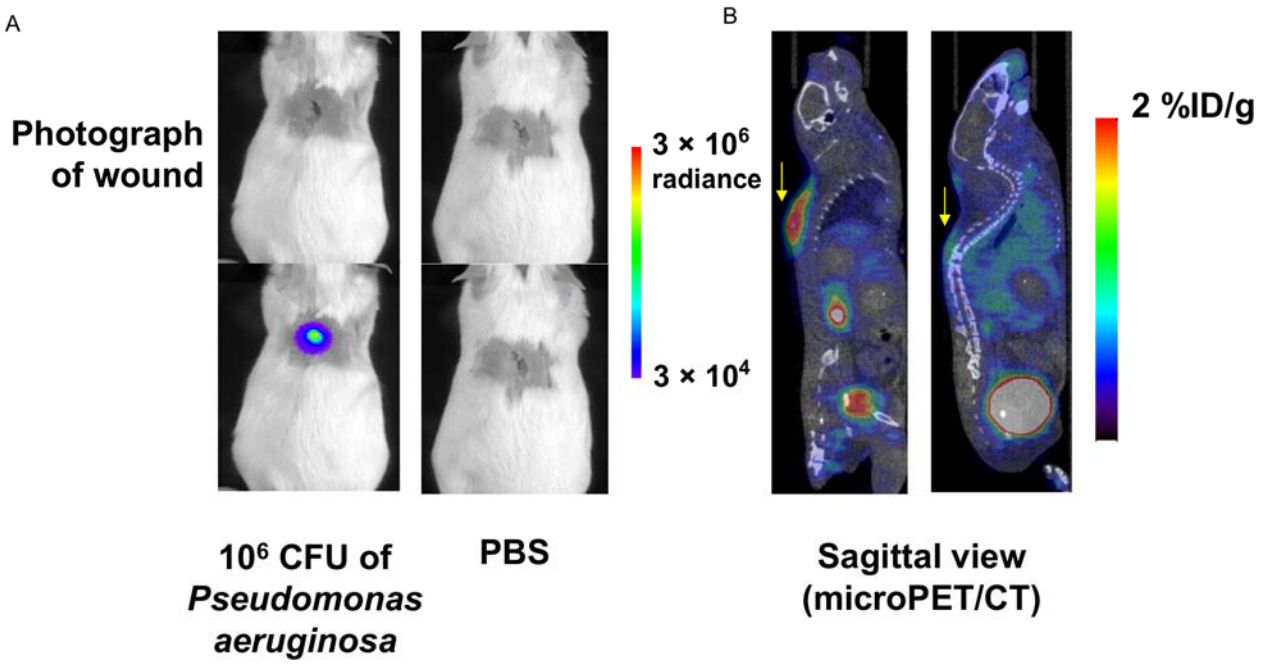

Figure 4: Evaluation of 6”-^{18}F-fluoromaltotriose in *Pseudomonas aeruginosa* wound infection model: A) Bioluminescence images of CD1 mice bearing *Pseudomonas aeruginosa* infected wound (left panel) and control mice (right panel) B) Sagittal slices from micro PET/CT scan of the same mice1h after intravenous administration of 6”-^{18}F-fluoromaltotriose

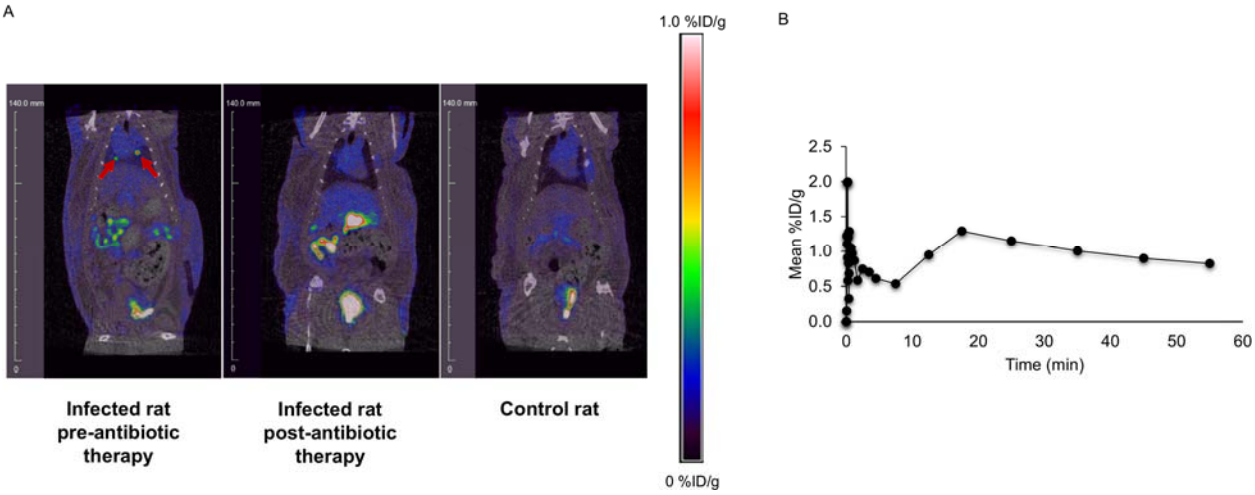

Figure 5: Evaluation of 6”-^{18}F-fluoromaltotriose PET/CT in a rat with an incidental infection post-cardiac surgery before and after antibiotic therapy: A) 6”-^{18}F-fluoromaltotriose microPET/CT images of the rat before (left panel) and after 1-month of antibiotic treatment (middle panel). Image is taken 1h after intravenous administration of 6”-^{18}F-fluoromaltotriose. The right panel shows a control rat that also received the tracer. There is virtually no uptake near the heart in the control rat. B) Time-activity curve of the hottest lesion in the infected rat before antibiotic therapy.

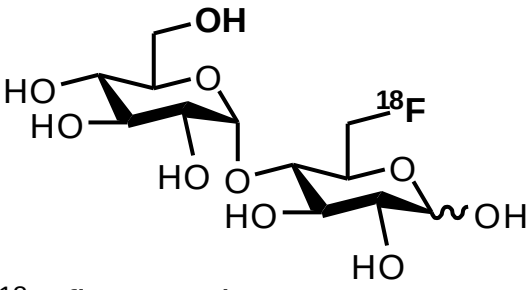

6- ^{18}F fluoromaltose

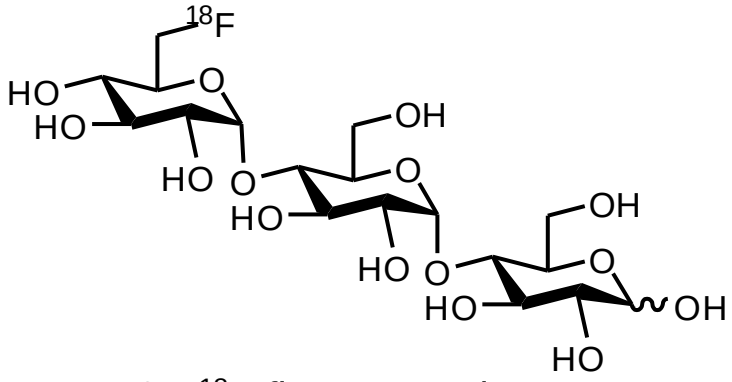

6”- ^{18}F fluoromatotriose

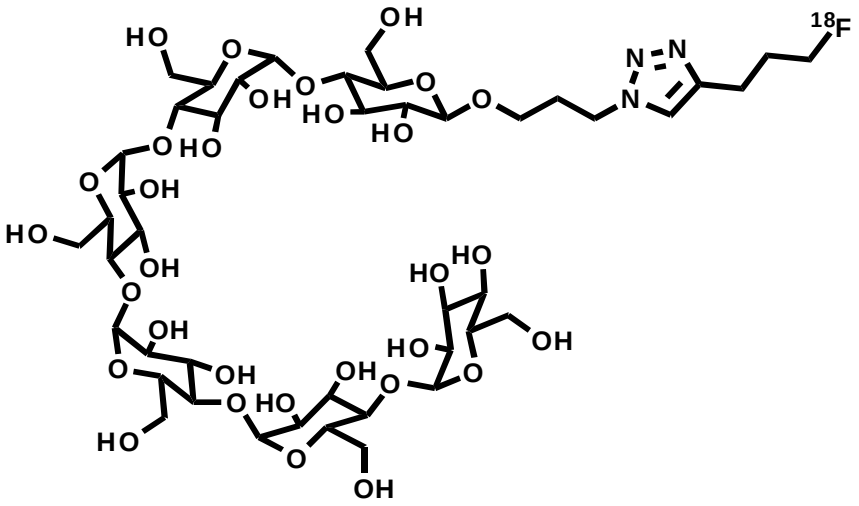

^{18}F-Fluoromaltohexose

Supplementary figure 1: Scheme showing the structures of the three different tracers targeting the maltodextrin transporter

Supplementary figure 2

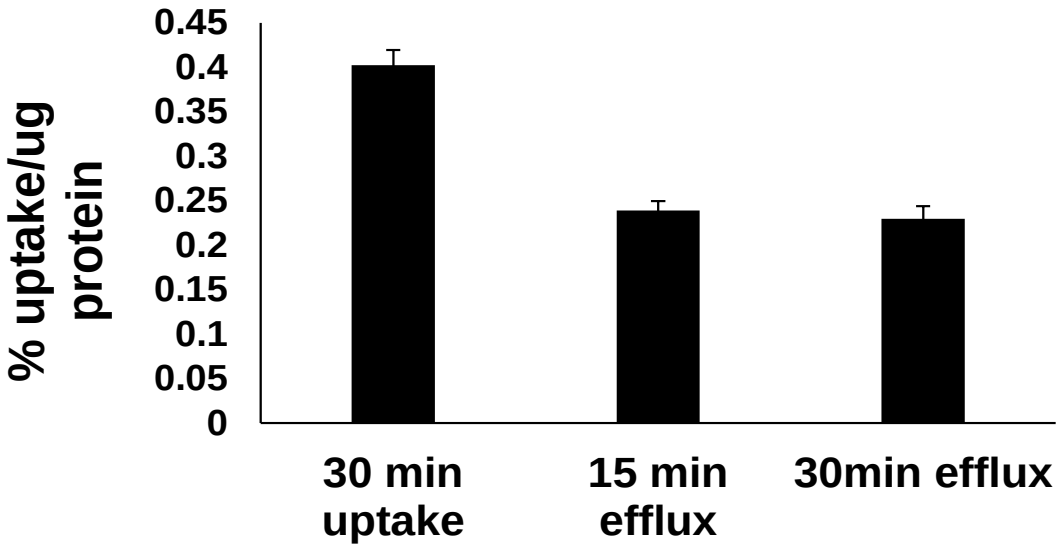

Supplementary figure 2: Efflux of 6”-^{18}F-fluoromaltotriose at 15 minutes and 30 minutes, following an initial 30 minutes incubation with the tracer. Error bars represent standard deviation

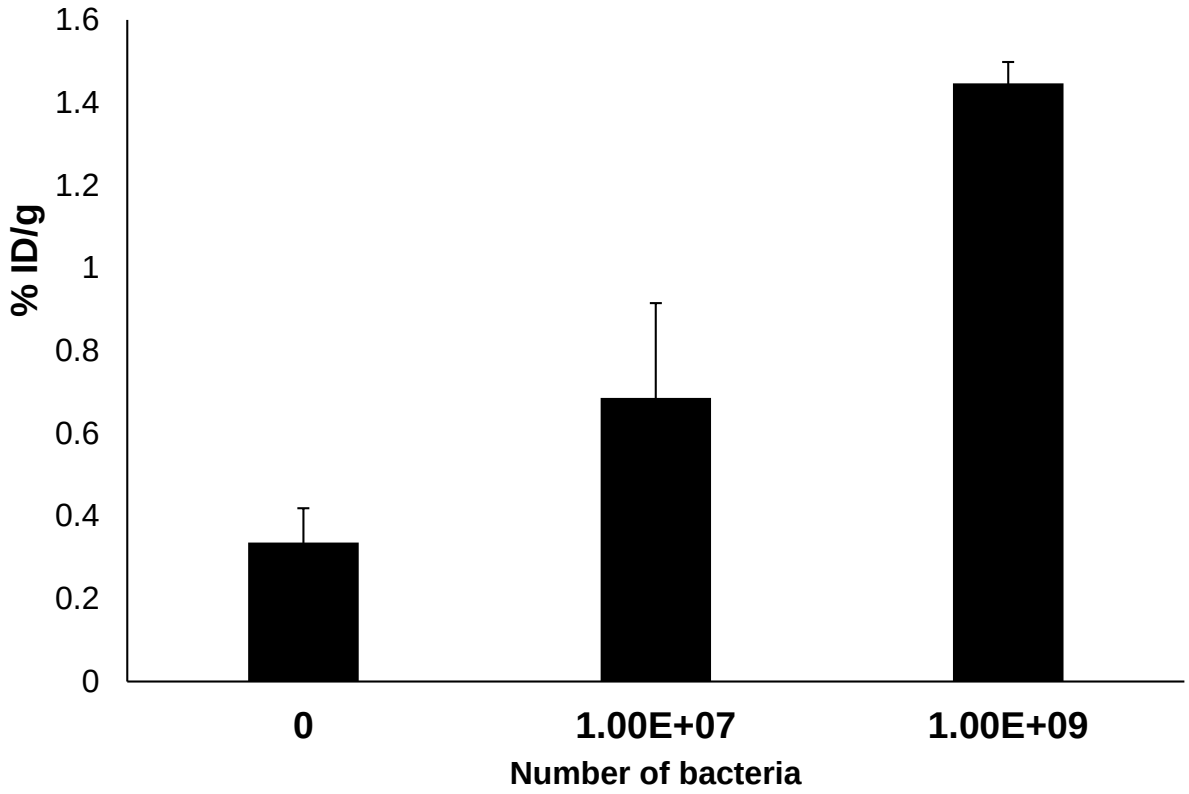

Supplementary figure 3: Ex-vivo bio-distribution showing the uptake of 6”-^{18}F-fluoromaltotriose in nude mice bearing different number of implanted *E.coli* (n=3 for each time point) 1h after administration of tracer. Error bars represent standard deviation.

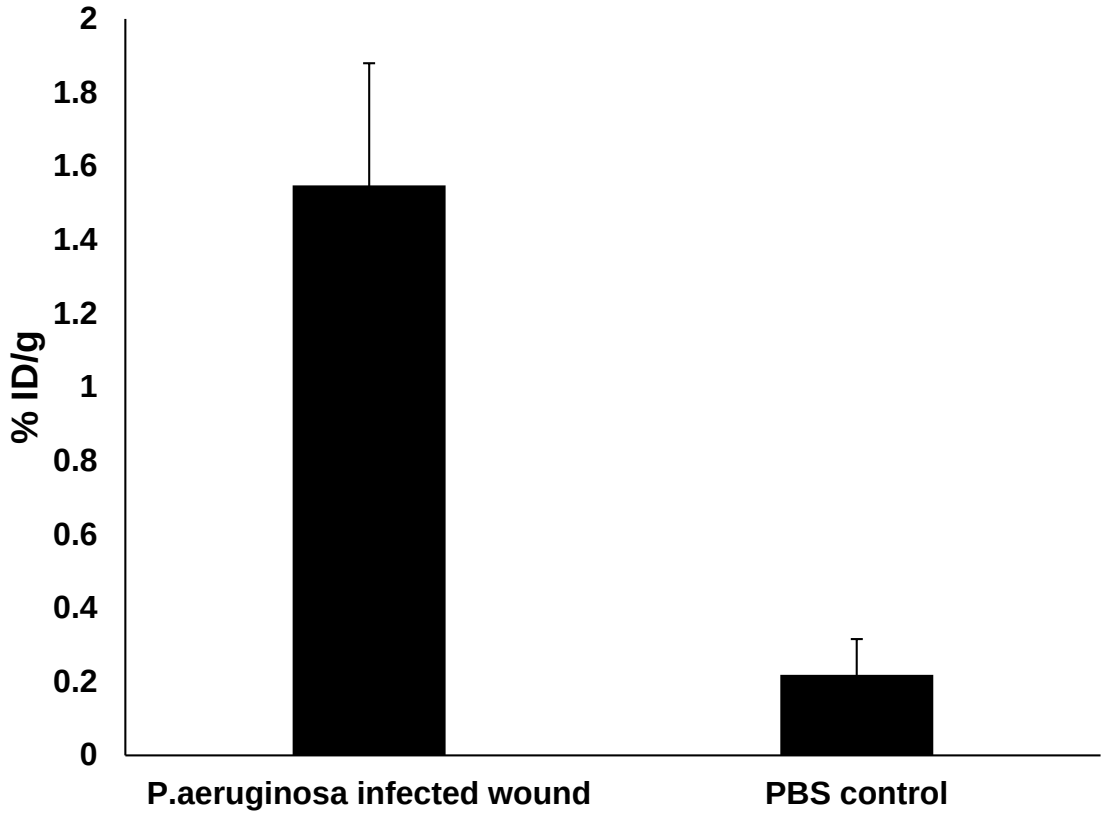

Supplementary figure 4: Ex-vivo biodistribution showing the uptake of 6”-^{18}F-fluoromaltotriose in *Pseudomonas aeruginosa* infected wounds (n=6) versus wounds in the control mice (n=3). Error bars represent standard deviation.

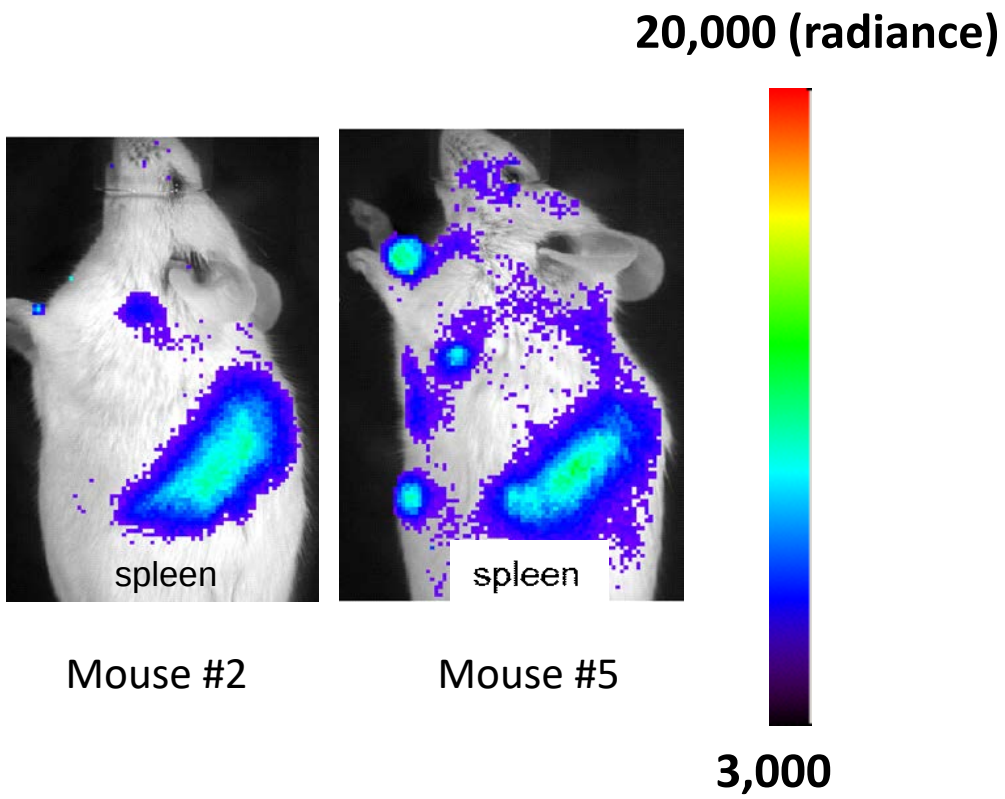

Supplementary figure 5: Bioluminescence imaging of mice 24h after the intravenous administration of 2 x 10^5 CFU of Xen 32, a bioluminescent strain of *Listeria monocytogenes*

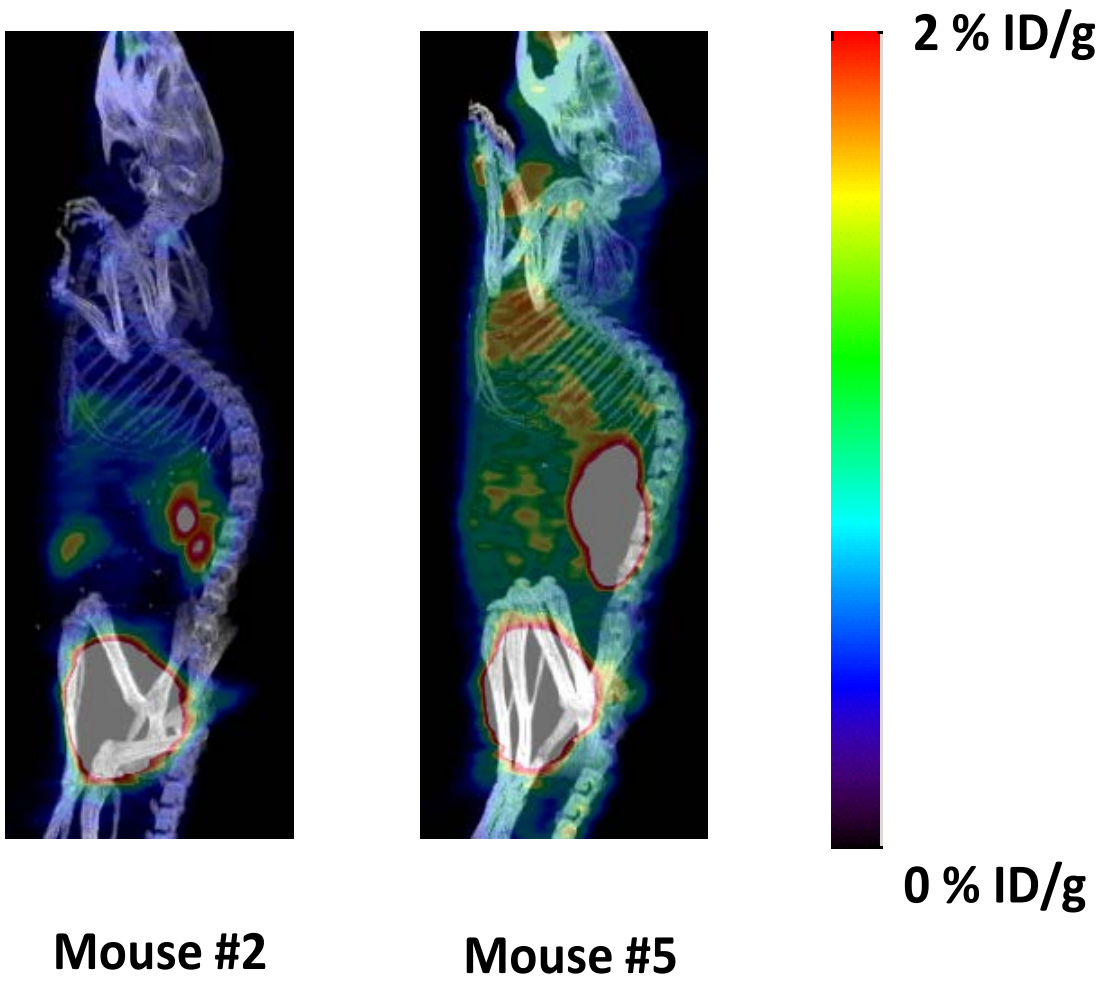

Supplementary figure 6: Maximum intensity projections from microPET/CT scans, of the same mice shown in supplementary figure 5, 1h after the injection of 7.4MBq of 6”-^{18}F-fluoromaltotriose.

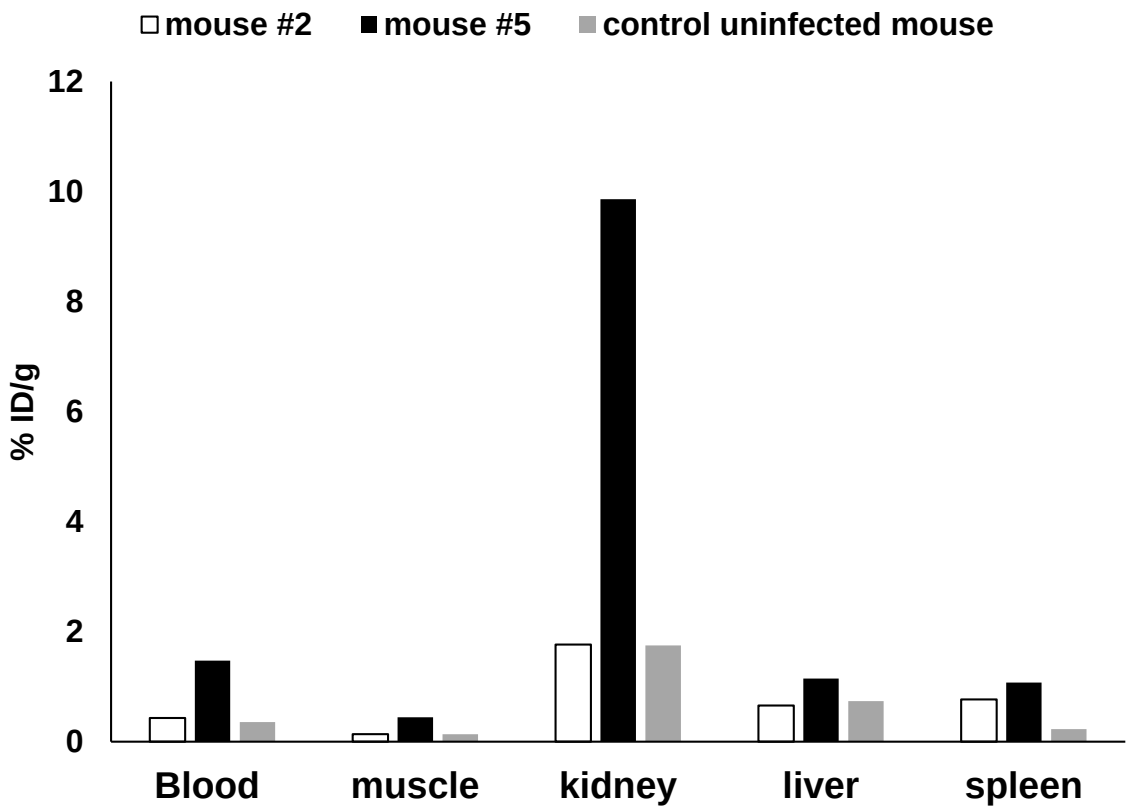

Supplementary figure 7: Ex vivo biodistribution of the same mice shown in supplementary figure 5 and 6, showing the uptake of 6”-^{18}F-fluoromaltotriose in the blood, kidney and spleen